SAND2018-10172J

Effect of fragile speckle patterns on accuracy of digital volume correlation

Brendan P. Croom[1], Helena Jin[2*], Bernice Mills[2], Xiaodong Li[1*]
[1] University of Virginia, Department of Mechanical and Aerospace Engineering, 122 Engineer's Way, Charlottesville, VA, 22904, USA
[2] Sandia National Laboratories, P.O. Box 969, Livermore, CA, 94551, USA
[*] Corresponding authors: hjin@sandia.gov, xl3p@virginia.edu

Abstract

Due to challenges in generating high-quality 3D speckle patterns for Digital Volume Correlation (DVC) strain measurements, DVC experiments often utilize the intrinsic texture and contrast of composite microstructures. One common deficiency of these natural speckle patterns is their poor durability under large deformations, which can lead to decorrelation and inaccurate strain measurements. Using syntactic foams as a model material, the effects of speckle pattern degradation on the accuracy of DVC strain measurements are assessed with both experimentally-acquired and numerically-generated images. It is shown that measurement error can be classified into two regimes as a function of the number of markers that have disappeared from the speckle pattern. For minor levels of damage beneath a critical level of damage, strain error remained near the noise floor of less than 100 $\mu\varepsilon$; above this level, error rapidly increased to unacceptable levels above 10,000 $\mu\varepsilon$. This transition occurred after 30%-40% of the speckles disappeared, depending on characteristics of the speckle pattern and its degradation mechanisms. These results suggest that accurate DVC measurements can be obtained in many types of fragile materials despite severe damage to the speckle pattern.

Keywords: Digital volume correlation, Error assessment, Syntactic foams, Decorrelation, Speckle pattern

1. Introduction

Both digital image correlation (DIC) [1] and its three-dimensional analogue digital

volume correlation (DVC) [2] compute the deformation field by tracking the aggregate motion of neighborhoods of features through a sequence of *in situ* experimental images (or 3D tomograms acquired by volumetric imaging techniques). This is achieved by dividing the measurement region of interest into subsets (subvolumes), and computing the translation, rotation and deformation of each subset (subvolume) from the reference state into the deformed state. Generally speaking, the sample should exhibit a high-quality, high-contrast, random "speckle pattern" to ensure the uniqueness and accuracy of the deformation measurement. One of the fundamental assumptions of DIC and DVC algorithms is that the individual speckles in the pattern be ***durable*** to allow them to be tracked in each image, so they should not substantially change appearance or disappear throughout the experiment. While such a speckle pattern can readily be applied to the surface of a specimen using spray paint, toner, or one of many other techniques for two-dimensional or stereo DIC, it is intrinsically challenging (and often undesirable) to modify the internal microstructure of three-dimensional specimens to meet these criteria for DVC measurement [3]. Instead, the intrinsic contrast and texture of the microstructure often substitutes for a high-quality artificial pattern.

As a result, a common deficiency of volumetric speckle patterns is the degradation of the microstructure under load, which can lead to decorrelation and inaccurate measurements. One common example is due to the development of damage in the material, which introduces new contrasting features to the material that were not present in the reference state. This is frequently encountered in brittle materials that undergo microcracking, such as ceramic matrix composites [4–7], plasterboard [8], and graphite [9]. Alternatively, this can be observed in the rupture of ductile metals, which is commonly preceded by void initiation, coalescence and growth into a crack [10]. Unless the damage mechanisms are explicitly incorporated into the warping functions

for the DVC algorithms (such as Heaviside DVC [11] or extended-DVC analogous to X-FEM techniques [12]), these features cause the image to violate the principle of "gray-level conservation" and therefore reduce the quality of the DVC measurement. However, it is generally acknowledged that DVC measurements will remain reasonably accurate provided the volume of damaged material remains small compared to the quantity of markers in the speckle pattern, as is the case in these examples.

Another scenario is the disappearance of individual speckles between the reference and deformed states, which also deleteriously affects DVC accuracy. This is particularly relevant for DVC experiments that tend to rely on the intrinsic texture of the material of interest, which may not be stable at large deformation as in the cases of foams [13–15], bone [2, 16] and granular materials [17, 18]. Even in surface-based DIC applications where artificial patterns are easily applied, the pattern may degrade when painted markers flake off the area of interest or fade with large deformation. It is currently unclear how this degradation affects DVC accuracy.

Unexpectedly, recent *in situ* X-ray Computed Tomography (XCT) experimental measurements by the authors have shown that DVC remains viable even in cases of severe damage to the speckle pattern with only minor losses in accuracy. Tomograms of syntactic foams were acquired at increasing levels of uniaxial compression [CROOM CITATION]. The syntactic foam consisted of an elastomer matrix filled with hollow glass microballoons (GMBs), which produced an archetypal 3D speckle pattern in the undamaged state (Fig. 1a). At increasing deformation, many of these GMBs crushed under mechanical load and eventually disappeared from the tomogram (Fig 1b-c), so a significant fraction of the markers that constituted the speckle pattern eventually disappeared from the images. Remarkably, accurate DVC measurements were obtained when up to 40% of the GMBs had collapsed.

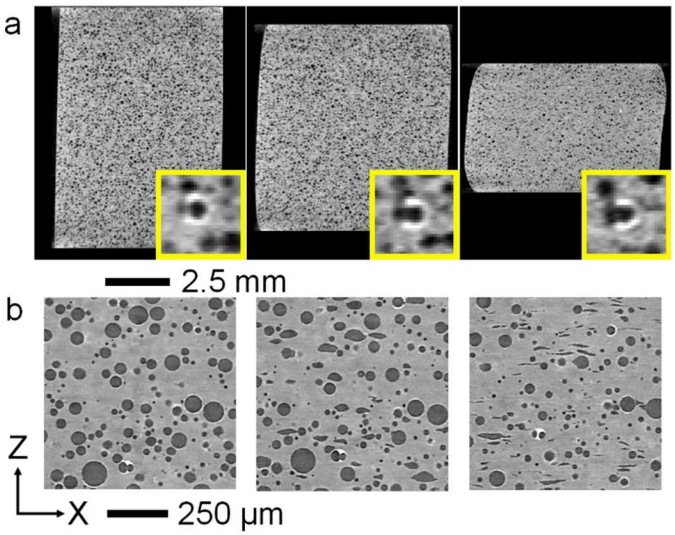

Fig. 1. Virtual cross-sections of compressed syntactic foam during *in situ* experiment. (a) Slices from low-resolution for DVC analysis at increasing strain, with insets showing subvolume size. (b) Slices from the corresponding high-resolution XCT images, showing collapse of GMBs.

The ability to correlate heavily damaged tomograms with DVC strongly contradicts our current assumptions about requirements for speckle patterns. The previous experiments [CROOM CITATION] clearly indicated that rules about gray level conservation can be relaxed in certain cases to permit measurement of specimens with fragile speckle patterns. Accordingly, DVC may be applicable to a much broader class of materials with non-durable microstructures than previously thought.

The objective of this paper is to explore the limits of DVC for materials with fragile microstructures and speckle patterns, and to quantify the effects of microstructure degradation on measurement accuracy. This has never been explored for conventional 2D-DIC, stereo-DIC or DVC. Certainly, use of DVC to study fragile microstructure comes at a cost of decreased accuracy, but how much damage is tolerable? The feasibility of DVC in these scenarios is first explored from a theoretical perspective, and then through experimental measurements using rigid body motion experiments to capture the effect on error under real imaging conditions. Finally, analysis of synthetic images with controlled levels of speckle pattern degradation is used to more

accurately understand the effects on DVC accuracy.

2. *Theory*

The basis for all DVC algorithms is the cross-correlation between the reference and deformed subvolumes. Since cross-correlation measures the similarity between two volumes, the optimal solution is obtained when each pixel in the deformed volume is mapped to the corresponding pixel in the reference coordinate, *i.e.* the displacement field is solved. One way of achieving this is by using optimization schemes to maximize the zero-mean, normalized cross-correlation (ZNCC), which is notably insensitive to systematic changes in contrast and illumination [19]. The ZNCC is computed as,

$$C_{ZNCC}(\boldsymbol{x}) = \frac{1}{N} \sum_{\boldsymbol{x} \in S} \left(\frac{F(\boldsymbol{x}) - \bar{F}}{\sigma_F} \frac{G\big(\boldsymbol{x} + \boldsymbol{u}(\boldsymbol{x})\big) - \bar{G}}{\sigma_G} \right) \tag{1}$$

where F and G correspond to the reference and deformed images, $\boldsymbol{x}$ represents the coordinates within the reference subset S, $\boldsymbol{u}(\boldsymbol{x})$ is the displacement field that maps undeformed coordinates into their deformed state, $\bar{F}$ and $\bar{G}$ indicate the average intensities of each subset, and σ_F and σ_G are the standard deviations of intensities within each subset. A high correlation score $C_{ZNCC} \rightarrow 1$ would indicate a strong match between the two specimens, implying that the physical displacement field has been accurately measured. The strain field can then be obtained through the spatial derivatives of $\boldsymbol{u}(\boldsymbol{x})$.

2.1. *Effects of fragile microstructure on DVC*

The primary concern about correlating images of fragile speckle patterns is that C_{ZNCC} will decrease as the specimen degrades, increasing the possibility that the optimization algorithm will identify inaccurate displacement and strain fields due to decorrelation effects. Thus, the

effects of fragile speckle patterns on the accuracy of DVC strain measurements can be demonstrated through changes in ZNCC (Eq. 1) as a function of degradation. For purposes of this paper, unique notation is developed to concisely describe the damaged character of speckle patterns:

- ϕ – Volume fraction of markers in undamaged state (from 0 to 1)
- α – Fraction of markers that are damaged (from 0 to 1)
- C – Residual contrast of all damaged markers (from 0 to 1)

To study these effects, two sets of 2D synthetic images of size 384^2 pixels (Fig. 2a) were generated according to the methods described in the later section **Generation of Synthetic Images**. In the first set, individual markers were damaged by a "fading" technique. In the second, the width of the markers was "shrunk" in proportion to the speckle damage. While both sets of images were identical in the undamaged and fully damaged states, the intermediate states were somewhat different. The undamaged images included an areal speckle fraction of $\phi = 0.26$. Half of the markers ($\alpha = 0.5$) were flagged for damage, while the other half of the speckles remained unchanged in the degraded images. The contrast C was reduced incrementally between images, which approximates the collapse of GMBs in the syntactic foam.

Results of the simulation in Fig. 2b indicated that the two damage mechanisms both reduced ZNCC nonlinearly, which would increase measurement error in DVC. Remarkably however, ZNCC remained above 0.9 for $C \geq 0.5$. In this context, it seems reasonable that DVC measurements can tolerate minor degradation to the speckle pattern, but become increasingly sensitive to subsequent damage.

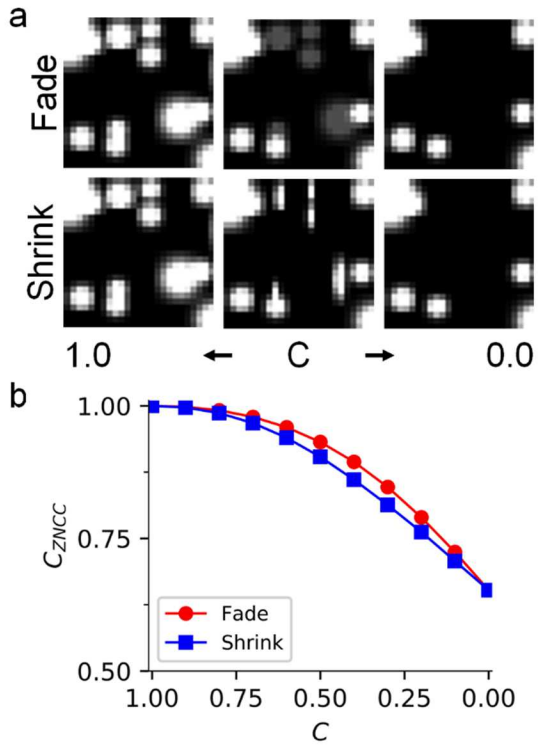

Fig. 2. Effect of "Fade" and "Shrink" speckle degradation mechanisms on DVC. (a) Schematic of the two mechanisms. (b) Resulting ZNCC scores as function of residual contrast C. $\alpha = 0.5$ of speckles were flagged for damage.

3. Experimental Methods

3.1. Materials

Sylgard GMB specimens were prepared by mixing A16 glass microballoons (3M) into two-part Sylgard 184 silicone elastomer (Dow Corning) and curing agent. The mixture was drawn into a cylindrical syringe and cured at room temperature with an accelerator. After curing, the molded foam was carefully cut into cylindrical specimens with 7 mm height and diameters of 4.8 mm. The diameter of A16 GMBs ranges from 30 to 95 μm within 10-90% distribution, with a mean diameter of 60 μm. Three specimens were manufactured with GMB volume fractions of 0.147, 0.225 and 0.422.

3.2. Rigid Body Motion Experiments

Experimental assessment of the error due to fragile specimens was performed using rigid

body motion experiments during an *in situ* compression experiment of the syntactic foams. Syntactic foam specimens were compressed uniaxially using a custom, screw-driven loading stage as reported in [4, 20]. The specimen was deformed between two acrylic platens to minimize reconstruction artifacts near the specimen edges. Each specimen was compressed in roughly 500 μm increments until DVC failed to achieve correlation, resulting in 5 or 6 *in situ* load steps per specimen.

Three tomograms were acquired at each load step. First, one high-resolution tomogram with voxel resolution of $[1.7\ \mu m]^3$ was used to quantify the volume fraction of GMBs in the undamaged state, and the fraction of damaged GMBs in subsequent steps. Second, a low-resolution tomogram was acquired with voxel resolution of $[8.5\ \mu m]^3$, resulting in a typical speckle diameter of 6-8 voxels that was ideal for DVC analysis. Finally, an additional low-resolution tomogram was acquired after axially displacing the sample 250 μm. The higher resolution tomogram was necessary to accurately measure the size and Feret shape (3D aspect ratio) of the GMBs [21], while the difference in measured strains between the pair of low-resolution tomograms yielded an assessment of DVC error. All tomographic imaging was performed using X-Radia MicroXCT 200 with X-ray source parameters 80 keV and 8 W. High-resolution tomograms were reconstructed from a set of 2401 radiographs between -103° and 103° rotation with 6.5 second exposure, and the low-resolution tomograms were reconstructed from a set of 1401 radiographs between -103° and 103° rotation with 7 second exposure.

Dimensional quantification of the GMBs was performed using Python image processing scripts and Avizo Fire 9.0. The raw 16-bit high-resolution tomograms were sequentially smoothed using nonlocal means filters, down sampled to 8-bit images, thresholded and segmented with standard image processing techniques. The 3D Feret shape was used to identify

the collapse of each segmented GMB, where FS > 1.3 indicated an ellipsoidal geometry consistent with GMB collapse. In contrast, low FS indicated spherical geometry of an intact GMB. Both the mechanical response and the damage behavior are reported in Fig. 3 for the three different volume fractions. GMB collapse occurred more rapidly for higher volume fractions due to stronger interactions between adjacent particles.

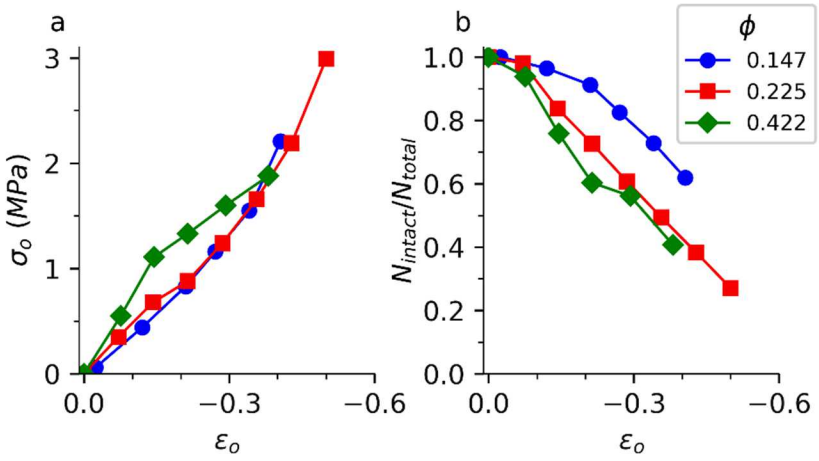

Fig. 3. Mechanical behavior of syntactic foam specimens. (a) Engineering stress vs. engineering strain curves. (b) Fraction of intact specimens vs. engineering strain.

The low-resolution tomograms were correlated against a single reference tomogram using commercial DVC code (Vic-Volume, Correlated Solutions) with a subset size of 29 voxels, step size of 10 voxels, and strain filter size of 5 subsets, resulting in a virtual strain gage size of [79 voxels]^3 = [672 μm]^3. All analysis was performed with a 4-tap spline-based interpolation scheme [19]. To measure the error in the DVC-computed strain, the difference in measured strain was recorded at each subset for the corresponding deformed and deformed rigid body motion tomograms.

4. Experimental Results

To experimentally evaluate the strain error, the DVC measurements were compared before and after rigid body motion. Since both tomograms were acquired at the same state of

compression and were correlated independently against the same reference tomogram, they should theoretically exhibit the same strain field. Any differences are attributed to the various sources of measurement error. In particular, error in the undeformed state ($\varepsilon = 0$) reflects the noise floor of the measurement system, while subsequent increases in error as the syntactic foam is compressed can be attributed to the effects of speckle pattern degradation.

Under uniform axial compression, the specimen exhibited strong variation in axial strain due to heterogeneous collapse of GMBs (Fig. 4). As was previously discussed in [CROOM GMB CITATION] and also observed in some other syntactic foams [22], this behavior was mechanistically related to the redistribution of stress around collapsed GMBs and the propagation of damage through the syntactic foam. For the specimen with volume fraction $\phi = 0.225$ of GMBs, the intensity of the strain field variation increased from $\varepsilon_{zz} \approx 0.01$ at a nominal strain of $\varepsilon_0 = -0.12$, to $\varepsilon_{zz} \approx 0.05$ at a nominal strain of $\varepsilon_0 = -0.30$ (Fig. 4a).

However, similar spatial patterns of artificial strain could be erroneously produced by DVC algorithms, so careful error assessment was required to verify the accuracy of this result. The banded strain behavior was determined to be physically accurate due to similarity in ε_{zz} and ε_{zz}^{RBM} results, where ε_{zz}^{RBM} was the measured strain after rigid body motion. In fact, variation between the measured strain before and after rigid body motion was too subtle to be discerned at the same scale as the strain field (Fig. 4b).

To more precisely evaluate the error, the difference between measured strain fields, $\Delta\varepsilon_{zz} = \varepsilon_{zz} - \varepsilon_{zz}^{RBM}$, was computed at each subvolume (Fig. 4c). Here, while the $\Delta\varepsilon_{zz}$ field exhibited a similar banded appearance, the magnitude of variation in $\Delta\varepsilon_{zz}$was roughly 5 times smaller than the variation in ε_{zz}. This trend was especially true when the specimen was imaged at low strain with little degradation to the speckle pattern ($\varepsilon_o = -0.12$). In the low-strain images,

variation approached the noise floor associated with this particular combination of XCT imaging and DVC analysis parameters. At higher strains ($\varepsilon_o = -0.30$) with more damage, the error increased marginally, although many subvolumes produced obviously spurious strain values with $|\Delta\varepsilon_{zz}| > 0.01$; these points appeared as yellow or purple spots in Fig. 4c. This trend was validated by comparing the histograms of $\Delta\varepsilon_{zz}$ in Fig. 4d, which showed both an increase in both standard deviation and number of outliers in each measured strain field. Interestingly, the increase in strain error occurred rapidly, as error at an intermediate strain of $\varepsilon_o = -0.24$ remained small.

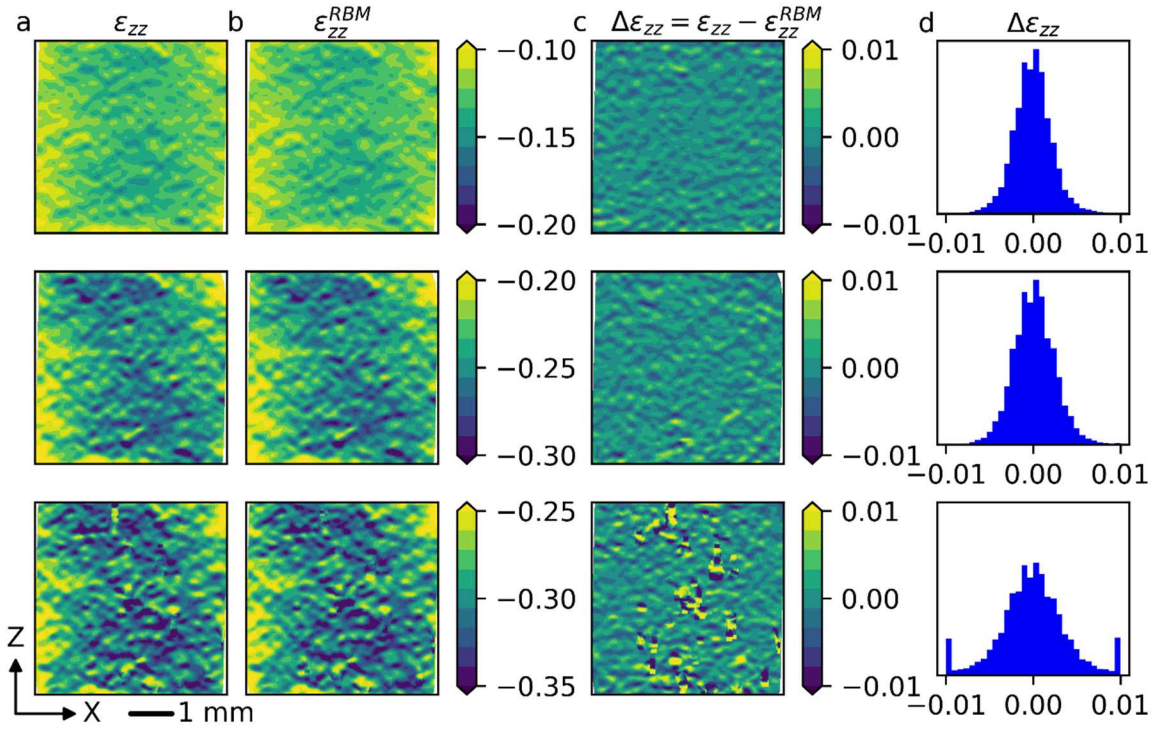

Fig. 4. Experimental assessment of strain error for syntactic foam specimen with $\phi = 0.223$. (a-b) Measured axial strain (a) before and (b) after rigid body motion; (c) difference between measured strain $\Delta\varepsilon_{zz}$; and (d) histogram of $\Delta\varepsilon_{zz}$. Results are shown at (top) nominal strain $\varepsilon_0 = -0.12$, (middle) $\varepsilon_o = -0.24$, and (bottom) $\varepsilon_0 = -0.30$.

Similar analyses were repeated for all three specimens, and the standard deviation of $\Delta\varepsilon_{zz}$ as a function of the speckle pattern degradation is reported for each load increment in Fig. 5.

These trends unequivocally showed that the accuracy of the DVC strain measurements remained near the measurement noise floor until a critical level of speckle pattern degradation was achieved, and was thus insensitive to small levels of GMB collapse. Typical error in this regime of minor speckle pattern degradation ranged from $\sigma_{\Delta\varepsilon_{zz}} = 98\ \mu\varepsilon$ for $\phi = 0.147$ and $54\ \mu\varepsilon$ for $\phi = 0.422$, with the different speckle pattern densities accounting for the discrepancies between specimens. Thus, DVC measurements could be considered "stable" beneath this critical level of degradation.

In contrast, error in the strain measurement rapidly grew to unacceptable levels once the speckle pattern degradation reached a critical value; at high levels of degradation, the measurement became "unstable". Due to volume-fraction dependent damage mechanisms for the syntactic foams, this transition varied somewhat between specimens. This transition occurred most rapidly at $\varepsilon_o = -0.2$ in the high volume fraction specimen, and later at $\varepsilon_o = -0.35$ in the low volume fraction specimen.

When measured in terms of damage to the speckle pattern, the results suggested that the critical level of degradation varied with both the GMB content and the damage mechanisms in the syntactic foam. For instance, the low volume fraction specimen exhibited the least resilience to speckle pattern damage with critical $\alpha \approx 0.27$ before error rapidly increased, which could be attributed to the sparse speckle pattern. On the other hand, the two specimens with higher volume fractions exhibited a critical $\alpha \approx 0.36$, indicating the benefit of a denser speckle pattern. Despite this, error increased faster in the $\phi = 0.422$ specimen after the critical transition, possibly due to enhanced strain localization.

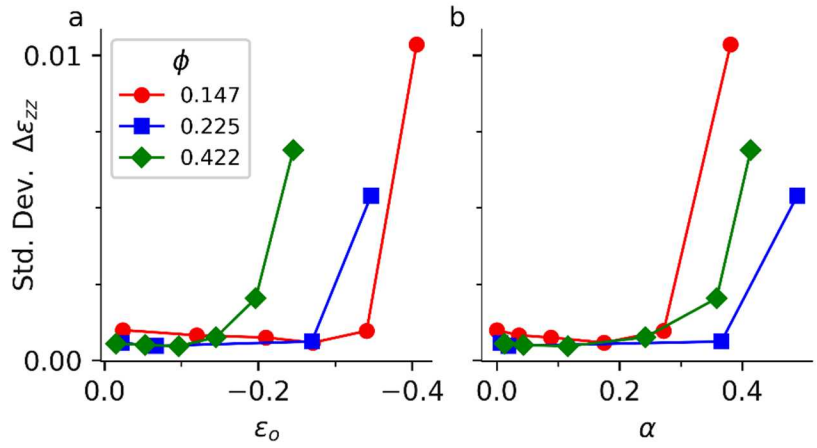

Fig. 5. Strain error as function of (a) engineering strain ε_o and (b) fraction of damaged GMBs α in the different syntactic foams.

5. Numerical Methods

While the experimental results clearly showed that accurate DVC measurements could be obtained despite widespread damage to the speckle pattern, these trends were convoluted by imaging artifacts such as distortion and other XCT error sources [23]. Additionally, heterogeneous deformation such as crush-band effects or strain localization [22] could further bias these measurements.

To address these challenges, synthetic images were generated and then analyzed by DVC to assess the separate roles of *fraction of damaged markers* and *degraded marker contrast* on the accuracy of DVC strain computations. These two parameters can approximate the degradation of many other materials in addition to syntactic foams. For example, while GMBs tend to quickly collapse and disappear from tomograms, other materials may exhibit a more gradual failure process in which markers slowly lose contrast. Simulations were performed for many volume fractions of markers. In this way, the simulation results can be readily adapted to other material systems.

5.1. Generation of Synthetic Images

To establish the effects of pattern degradation on DVC error, artificial images with increasing levels of degradation and no strain were generated. Synthetic images with prescribed damage levels were developed through a three-step process of generating an undamaged reference pattern, degrading selected markers in the pattern, and then adding Gaussian noise to simulate experimental image conditions. Correlation of the synthetic volumes to the undamaged reference state using commercial DVC software provided an assessment of errors due to microstructure degradation.

First, a reference volume of size $1024 \times 256 \times 256$ voxels was generated with bright markers on a dark background by perturbing the position of markers on a 3D regular grid, similar to the technique used in [24]. The grid pitch was modified to change the volume fraction ϕ between 0.136 and 0.407 which encompassed representative porosities found in many syntactic foams and other DVC specimens [22, 25–27]. Speckles were modeled as modified 3D Gaussian signals with standard deviations σ randomly selected between 1 and 3 voxels,

$$I(\boldsymbol{x}) = \min\left(200,400\, exp\left(\sum_{i=1}^{3} \frac{-(x_i - x_i^c)^2}{\sigma^2}\right)\right) \tag{2}$$

where x_i represents the image coordinate, and x_i^c represents the subpixel center of the marker. The intensity of the central region in each speckle was truncated to imitate the uniform intensity of the hollow GMBs. In contrast to explicitly modeling the spherical particles, the modified Gaussian profile allowed facile imposition of subpixel displacements and deformations without relying on downsampling or interpolation filters. The speckles in the deformed images were analytically translated by 0.5 voxels from their reference position.

To efficiently survey the different combinations of α and C that represent various degrees

of pattern degradation, damage was introduced to each pattern by randomly flagging markers for degradation as a linear function of the x coordinate. In this way, the probability of damage increased from $\alpha = 0.0$ at $x = 0$ to $\alpha = 1.0$ at $x = 1024$ (Fig. 6). The residual contrast of each flagged particle was incrementally decreased from $C = 1.0$ to 0.0, resulting in several images with many faint particles and one image with fully deleted particles. Since damage only varied in the x direction, there existed many data points on each $y - z$ plane to statistically analyze the effects of marker degradation. The intensities of the 3D volumes were scaled for 8-bit images, with the dark background assigned an intensity of 25, and the undamaged particles an intensity of 225; this intensity range allowed noise to be added to the image.

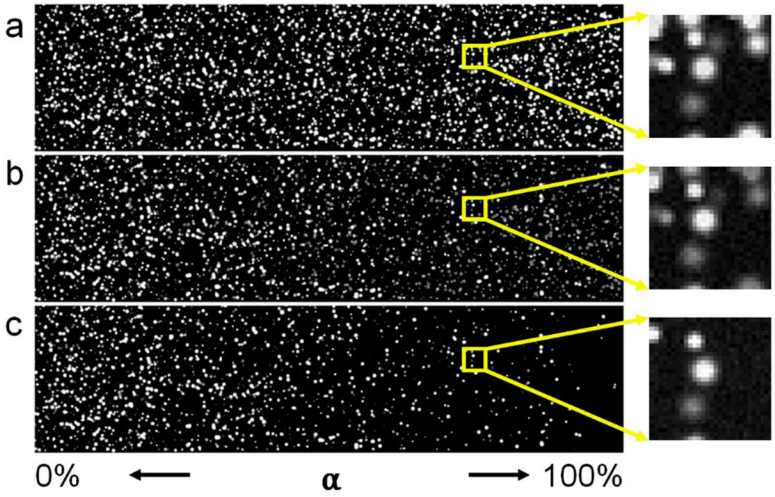

Fig. 6. Damage gradient in synthetic zero-strain images (a-c) Corresponding 2D slices with (a) $C = 1.0$, (b) $C = 0.5$, and (c) $C = 0.0$. Insets on right indicate subset size (29^3 voxels) used in DVC analysis, and highlight how selected markers gradually faded with decreasing C. $\phi = 0.137$.

Finally, Gaussian noise was independently added to each image to approximate error in the imaging conditions. X-ray tomograms typically exhibit higher levels of noise than 2D optical images, and this noise will limit the accuracy of the strain computation. We quantify noise using the Noise to Signal Ratio (NSR), defined as

$$NSR = \frac{\sigma_{noise}}{I_{max} - I_{min}} \quad (3)$$

where σ_{noise} is the standard deviation of the noise, and $I_{max} - I_{min}$ is the intensity range in the signal. Our experimental results using laboratory-based XCT equipment yielded tomograms with NSR of ~3%, whereas tomograms from synchrotron or more modern XCT systems could produce lower noise levels. A sensitivity study found that error in strain computation due to NSR remained below 0.0001, which was insignificant relative to the effect of a fragile speckle pattern (with $\sigma_\varepsilon \approx 0.001 - 0.01$). Therefore, simulations were performed with a representative NSR of 3%.

DVC analysis was performed using the commercial Vic-Volume DVC software (Correlated Solutions) with parameters that matched the experimental error analysis (subset size of 29^3 voxels and step size of 10 voxels). These parameters resulted in ~50,000 subsets per volume, and 529 subsets for a given fraction of damaged markers. Lagrangian strain was computed at each subset. Strain was computed using a filter of size 5^3 subsets, which was the minimum amount of filtering available in the Vic-Volume software.

6. Numerical Results

Analysis of the zero-displacement simulations clearly revealed that the average marker volume fraction ϕ, the fraction of damaged markers α, and the residual contrast of damaged markers C strongly influenced the accuracy of the strain computation, as summarized in Fig. 7. Results are presented for three different volume fractions that corresponded to those used in the experiments, and error is defined as the standard deviation of the measured artificial strain.

Similar to the experimental results, there appeared to exist two domains for strain computation. During the initial stable computation regime, strain error increased linearly with respect to α. This continued until a critical damage value was reached, after which the

computation became unstable and error increased rapidly. Below the critical level of speckle pattern degradation, the strain error increased gradually with α but remained relatively small; in the worst-case scenario with $\phi = 0.137$ and $C = 0.0$, the error remained less than 0.0025 (250 $\mu\varepsilon$) throughout the stable DVC regime. The transition into the unstable regime is identified by the inflection point in the plots, which varied with ϕ and C; values of this transition point (for $C = 0.0$) ranged from $\alpha = 0.48$ for $\phi = 0.137$, $\alpha = 0.60$ for $\phi = 0.217$, and $\alpha = 0.67$ for $\phi = 0.404$.

The magnitude of error in the stable measurement regime varied with the residual contrast of the damaged speckles C and the volume fraction of speckles in the image ϕ. In general, strain error improved with increasing ϕ and C. This was qualitatively consistent with the experiments, which also found that the high ϕ specimens exhibited a lower noise floor than low ϕ specimens.

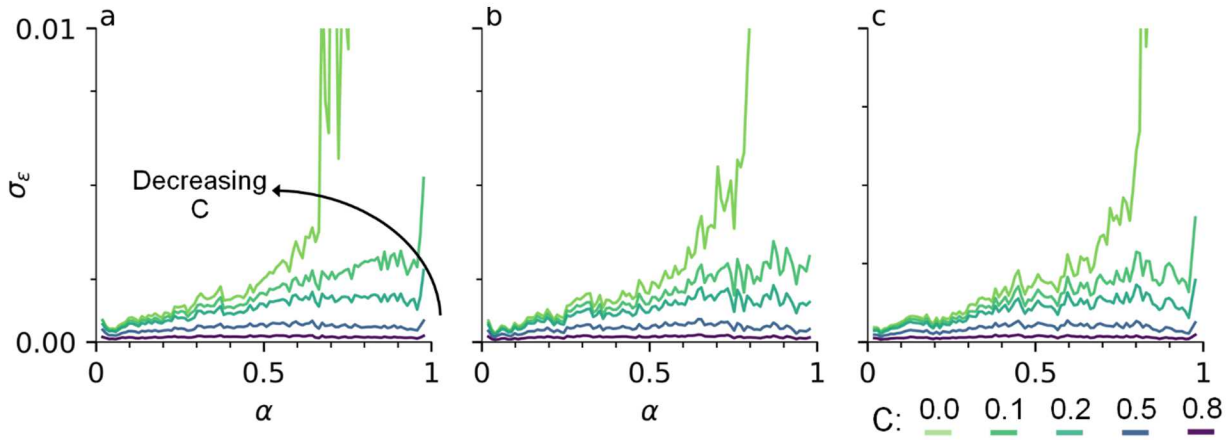

Fig. 7. Effect of speckle pattern degradation and volume fraction ϕ on strain error. (a-c) Results for ϕ of (a) 0.137, (b) 0.217, (c) 0.404. NSR = 3%.

7. Discussion

7.1. Comparison between experiment and numerical results

Most importantly, these results showed that accurate DVC measurements can be obtained

despite non-trivial levels of degradation to the speckle pattern. This was confirmed using both experimental tomograms and numerically-generated images with controlled levels of speckle pattern degradation. In both cases, DVC error remained small while below a critical level of degradation (*i.e.,* the stable measurement regime), after which strain error rapidly increased to unacceptable levels (unstable measurement regime). Thus, the transition between stable and unstable measurement regimes reflected the degradation of the speckle pattern rather than peculiarities of the syntactic foams used in experiments. Fundamentally, this appeared to be related to the effects of speckle pattern degradation on the correlation strength C_{ZNCC}. The nonlinear dependence of C_{ZNCC} on degradation allowed C_{ZNCC} to remain high after the disappearance of a small fraction of speckles, but C_{ZNCC} rapidly decreased with further degradation.

Despite this, several key differences were observed between the two analyses. First, DVC error analysis of the experimental and numerically-generated images revealed different trends within the stable measurement regime. In particular, the experimental results suggested a constant error of 50-100 $\mu\varepsilon$ for all levels of degradation beneath the critical value, while the numerical images suggested a *linearly increasing* error within this range (for constant C). The likely explanation of this trend was that the effective C for the collapsed GMBs was not constant but decreased throughout the experiment. Initially, the Feret shape of damaged particles would be small, such that the particle would be pseudo-spherical and would provide strong residual contrast C in the tomogram. Subsequent loading would further compress the particles, increasing Feret shape and decreasing C. At small deformations, the typical C would remain large enough to negligibly affect the error. For example, from Fig. 7 it was shown that strain error did not substantially increase with $C \approx 0.5$ regardless of the fraction of speckles damaged. This allowed

error to remain low when the GMBs were partially collapsed, but to rapidly increase as the damaged particles fully closed.

Second, analysis of the numerically-generated images predicted critical damage levels that were higher than those observed in the experiment. Plausibly, damage localization in the experiment contributed to the increased error. Detailed analysis of the tomograms showed that bands of elevated strain (visible in Fig. 4) corresponded to regions with clusters of crushed GMBs, such the speckle pattern damage would locally exceed the global average and therefore increase the measurement error. This behavior was caused by particle-to-particle interactions [28] and local clustering of GMBs [29], and was particularly severe in the high volume fraction specimens ($\phi = 0.422$ and to a lesser extent $\phi = 0.225$).

7.2. Implications

The ability to accurately correlate heavily damaged speckle patterns should enable DVC-based strain measurements in a broad class of materials with fragile microstructures, including syntactic foams and possibly many other materials. This was previously thought to be impossible or ill-advised at best, since it would violate the principle of gray-level conservation. In contrast, these results showed that roughly 30-40% of speckles could disappear before strain error noticeably worsened to $\Delta\varepsilon > 0.01$. We emphasize that in certain cases (*e.g.,* very large strains), even larger error could be tolerated.

The current findings were only obtained for particle-based speckle patterns, where damage resulted in the disappearance of particles in the pattern. Therefore, it remains unclear how other types of speckle patterns and damage mechanisms affect the stability of DVC measurements. Future work is required to assess this behavior in granular, foam or fibrous composites, and also materials that undergo different damage mechanisms such as microcracking

or cell collapse. Simulation of these effects using numerically generated images may prove a cost-effective manner to test viability of DVC measurement in these other materials.

Finally, these results demonstrate the importance of restricting DVC measurement to scenarios with sub-critical levels of speckle pattern degradation. For the current syntactic foam, this was achieved by relating damage to the uniaxial deformation, which was found to reliably correspond to DVC error across multiple samples with identical GMB volume fractions. Similar testing should be performed on other materials to avoid inaccurate strain measurements.

This becomes more challenging when damage is locally concentrated rather than homogeneously dispersed throughout the material, which would cause DVC error to increase more rapidly near the location of damage. While a straightforward but cautious approach would be to manually trim the region of interest around the damaged regions, this can be tedious and also disposes of many accurate correlation points. Since the speckle pattern degradation reduces the correlation strength, it may be possible to introduce automatic screening of each correlated subset. One intriguing avenue for evaluating the quality of the experimental strain measurement is to implement so-called q-factor DVC, which assesses the sharpness and uniqueness of the cross-correlation through image quality factors [30]. Q-factor DVC was originally developed for cases of large deformation, which causes round speckles to collapse into ellipses and is comparable to the collapse of GMBs in the syntactic foam. Additionally, this work can be integrated into the framework for incremental DIC/DVC techniques [31, 32] to indicate when the reference image should be updated.

8. Conclusions

Accurate DVC measurements were obtained during *in situ* testing of specimens with fragile microstructures even with widespread damage to the speckle pattern. This was validated

using experiments on three types of syntactic foams with different volume fractions of glass microballoon reinforcement, as well as analysis of numerically-generated images with controlled levels of speckle pattern degradation; in both cases, correlation succeeded despite large proportions of individual markers in the speckle pattern disappearing between the reference and deformed states up to 20-35% compression and 30-40% damaged speckles. These findings justify the use of DVC on many types of materials with unstable microstructures, including syntactic foams, ceramic composites, bone and others. From these analyses, the following conclusions are made:

- The performance of DVC as a function of speckle pattern degradation was classified into two regimes. Below a critical level of speckle degradation, DVC measurement was "stable" and error approached the experimental noise floor. The strain error was constant within this regime, and varied inversely with the speckle pattern density. Above this critical value, measurement became "unstable" and error rapidly increased with further degradation to the speckle pattern.
- The transition from stable to unstable measurement regimes typically occurred after 30-40% of the speckles were damaged. This critical value depended on several factors including pattern quality, marker volume fraction and the degree of damage localization. In particular, larger volume fractions of markers tend to stabilize the DVC measurements to accommodate more severe damage to the speckle pattern.
- The experimental trends were qualitatively replicated using numerically-generated images, which successfully captured the transition between stable and unstable measurement regimes. However, the numerical analysis tended to

overestimate transition between these two regimes, likely due to subtle differences in the damage mechanisms between the syntactic foam and the simulated images. Despite this, numerically-generated images may be used to preliminarily simulate the viability of DVC measurements in other types of fragile speckle patterns, such as those found in foams or fiber-reinforced composites.

Acknowledgements

This research is supported by Sandia National Laboratories and the National Science Foundation (NSF) Graduate Research Fellowship Program under Grant No. 1315231. Sandia National Laboratories is a multimission laboratory managed and operated by National Technology and Engineering Solutions of Sandia, LLC., a wholly owned subsidiary of Honeywell International, Inc., for the U.S. Department of Energy's National Nuclear Security Administration under contract DE-NA-0003525. This paper describes objective technical results and analysis. Any subjective views or opinions that might be expressed in the paper do not necessarily represent the views of the U.S. Department of Energy or the United States Government.

References

1. Sutton MA, Wolters W, Peters WH, et al (1983) Determination of displacements using an improved digital correlation method. Image Vis Comput 1:133–139 . doi: 10.1016/0262-8856(83)90064-1
2. Bay BK, Smith TS, Fyhrie DP, Saad M (1999) Digital volume correlation: Three-dimensional strain mapping using X-ray tomography. Exp Mech 39:217–226 . doi:

10.1007/BF02323555

3. Bay BK (2008) Methods and applications of digital volume correlation. J Strain Anal Eng Des 43:745–760 . doi: 10.1243/03093247JSA436

4. Croom BP, Xu P, Lahoda EJ, et al (2017) Quantifying the three-dimensional damage and stress redistribution mechanisms of braided SiC/SiC composites by in situ volumetric digital image correlation. Scr Mater 130:238–241 . doi: 10.1016/j.scriptamat.2016.12.021

5. Saucedo-Mora L, Lowe T, Zhao S, et al (2016) In situ observation of mechanical damage within a SiC-SiC ceramic matrix composite. J Nucl Mater 481:13–23 . doi: 10.1016/j.jnucmat.2016.09.007

6. Saucedo-Mora L, Mostafavi M, Khoshkhou D, et al (2016) Observation and simulation of indentation damage in a SiC-SiCfibre ceramic matrix composite. Finite Elem Anal Des 110:11–19 . doi: 10.1016/j.finel.2015.11.003

7. Mazars V, Caty O, Couégnat G, et al (2017) Damage investigation and modeling of 3D woven ceramic matrix composites from X-ray tomography in-situ tensile tests. Acta Mater 140:130–139 . doi: 10.1016/j.actamat.2017.08.034

8. Bouterf A, Maire E, Roux S, et al (2018) Analysis of compaction in brittle foam with multiscale indentation tests. Mech Mater 118:22–30 . doi: 10.1016/j.mechmat.2017.12.004

9. Barhli SM, Saucedo-Mora L, Jordan MSL, et al (2017) Synchrotron X-ray characterization of crack strain fields in polygranular graphite. Carbon N Y 124:357–371 . doi: 10.1016/J.CARBON.2017.08.075

10. Hild F, Bouterf A, Roux S (2015) Damage measurements via DIC. Int J Fract 191:77–105 . doi: 10.1007/s10704-015-0004-7

11. Valle V, Bokam P, Germaneau A, Hedan S (2018) New Development of Digital Volume Correlation for the Study of Fractured Materials. Exp Mech 1–15 . doi: 10.1007/s11340-018-0415-2

12. Rannou J, Limodin N, Réthoré J, et al (2010) Three dimensional experimental and numerical multiscale analysis of a fatigue crack. Comput Methods Appl Mech Eng 199:1307–1325 . doi: 10.1016/J.CMA.2009.09.013

13. Roux S, Hild F, Viot P, Bernard D (2008) Three-dimensional image correlation from X-ray computed tomography of solid foam. Compos Part A Appl Sci Manuf 39:1253–1265 . doi: 10.1016/j.compositesa.2007.11.011

14. Bouterf A, Roux S, Hild F, et al (2014) Digital volume correlation applied to X-ray tomography images from spherical indentation tests on lightweight gypsum. Strain 50:444–453 . doi: 10.1111/str12101

15. Pierron F, McDonald SA, Hollis D, et al (2013) Comparison of the mechanical behaviour of standard and auxetic foams by x-ray computed tomography and digital volume correlation. Strain 49:467–482 . doi: 10.1111/str.12053

16. Verhulp E, van Rietbergen B, Huiskes R (2004) A three-dimensional digital image correlation technique for strain measurements in microstructures. J Biomech 37:1313–1320 . doi: 10.1016/j.jbiomech.2003.12.036

17. Forsberg F, Siviour CR (2009) 3D deformation and strain analysis in compacted sugar using x-ray microtomography and digital volume correlation. Meas Sci Technol 20:095703 . doi: 10.1088/0957-0233/20/9/095703

18. Bornert M, Lenoir N, Bésuelle P, et al (2010) Discrete and continuum analysis of localised deformation in sand using X-ray μCT and volumetric digital image correlation.

Géotechnique 60:315–322 . doi: 10.1680/geot.2010.60.5.315

19. Sutton MA, Orteu J-J, Schreier HW (2009) Image Correlation for Shape, Motion and Deformation Measurements. Springer US, Boston, MA

20. Croom B, Wang W-M, Li J, Li X (2016) Unveiling 3D Deformations in Polymer Composites by Coupled Micro X-Ray Computed Tomography and Volumetric Digital Image Correlation. Exp Mech 56:999–1016 . doi: 10.1007/s11340-016-0140-7

21. Patterson BM, Escobedo-Diaz JP, Dennis-Koller D, Cerreta E (2012) Dimensional quantification of embedded voids or objects in three dimensions using X-ray tomography. Microsc Microanal 18:390–8 . doi: 10.1017/S1431927611012554

22. Adrien J, Maire E, Gimenez N, Sauvant-Moynot V (2007) Experimental study of the compression behaviour of syntactic foams by in situ X-ray tomography. Acta Mater 55:1667–1679 . doi: 10.1016/j.actamat.2006.10.027

23. Limodin N, Réthoré J, Adrien J, et al (2011) Analysis and Artifact Correction for Volume Correlation Measurements Using Tomographic Images from a Laboratory X-ray Source. Exp Mech 51:959–970 . doi: 10.1007/s11340-010-9397-4

24. Mazzoleni P, Matta F, Zappa E, et al (2015) Gaussian pre-filtering for uncertainty minimization in digital image correlation using numerically-designed speckle patterns. Opt Lasers Eng 66:19–33 . doi: 10.1016/j.optlaseng.2014.08.004

25. Lachambre J, Maire E, Adrien J, Choqueuse D (2013) In situ observation of syntactic foams under hydrostatic pressure using X-ray tomography. Acta Mater 61:4035–4043 . doi: 10.1016/j.actamat.2013.03.017

26. Patterson BM, Cordes NL, Henderson K, et al (2016) In situ X-ray synchrotron tomographic imaging during the compression of hyper-elastic polymeric materials. J

Mater Sci 51:171–187 . doi: 10.1007/s10853-015-9355-8

27. Gupta N (2007) A functionally graded syntactic foam material for high energy absorption under compression. Mater Lett 61:979–982 . doi: 10.1016/j.matlet.2006.06.033

28. Tagliavia G, Porfiri M, Gupta N (2011) Analysis of particle-to-particle elastic interactions in syntactic foams. Mech Mater 43:952–968 . doi: 10.1016/j.mechmat.2011.08.008

29. Yu M, Zhu P, Ma Y (2013) Effects of particle clustering on the tensile properties and failure mechanisms of hollow spheres filled syntactic foams: A numerical investigation by microstructure based modeling. Mater Des 47:80–89 . doi: 10.1016/j.matdes.2012.12.004

30. Landauer AK, Patel · M, Henann · D L, Franck · C (2018) A q-Factor-Based Digital Image Correlation Algorithm (qDIC) for Resolving Finite Deformations with Degenerate Speckle Patterns. Exp Mech 58:815–830 . doi: 10.1007/s11340-018-0377-4

31. Pan B, Dafang W, Yong X (2012) Incremental calculation for large deformation measurement using reliability-guided digital image correlation. Opt Lasers Eng 50:586–592 . doi: 10.1016/j.optlaseng.2011.05.005

32. Hu Z, Luo H, Bardenhagen SG, et al (2015) Internal Deformation Measurement of Polymer Bonded Sugar in Compression by Digital Volume Correlation of In-situ Tomography. Exp Mech 55:289–300 . doi: 10.1007/s11340-014-9856-4